ENERGETICS OF AN ACTIVE REGION OBSERVED FROM HELIUM-LIKE SULPHUR LINES

TETSUYA WATANABE[1], ALPHONSE C. STERLING[2,*], HUGH S. HUDSON[3] and LOUISE K. HARRA[4]

[1]*National Astronomical Observatory, 2-21-1 Osawa Mitaka, Tokyo 181-8588, Japan (e-mail: WATANABE@uvlab.mtk.nao.ac.jp)*

[2]*NASA/Marshall Space Flight Center, SD50/Space Science Department, Huntsville, AL 35812, U.S.A.*

[3]*Solar Physics Research Corporation, 4720 Calle Desecada, Tucson, AZ 85718, U.S.A.*

[4]*Mullard Space Science Laboratory, Holmbury St. Mary, Dorking, Surrey RH5 6NT, U.K.*

(Received 24 October 2000; accepted 8 February 2001)

Abstract. We report temperature diagnostics derived from helium-like ions of sulphur for an active region NOAA 7978 obtained with Bragg Crystal Spectrometer (BCS) on board the *Yohkoh* satellite. For the same region we estimate conductive flux downward to the chromosphere by the Coronal Diagnostic Spectrometer (CDS) on board the Solar and Heliospheric Observatory (SOHO) satellite. This region appeared as a region of soft X-ray enhancement in May 1996, underwent a period of enhanced activity coinciding with flux emergence between 6 July and 12 July, and then continued to exist in a nearly flareless state for several solar rotations until November 1996. Energy balance of the non-flaring active region is basically consistent with a model of an arcade of coronal loops having an average loop-top temperature of 4×10^6 K. Energy from flare activity during a period of flux emergence is comparable to the energy requirements of the non-flaring active region. However, the non-flaring energy is roughly constant for the subsequent solar rotations following the birth of the active region even after the flare activity essentially subsided. Energy partition between flare activity and steady active-region heating thus varies significantly over the lifetime of the active region, and active-region emission cannot always be identified with flaring.

1. Introduction

The solar active region NOAA 7978 was conspicuously active on the solar disk in July 1996. It developed out of an activity complex visible since May 1996, showed a rapid growth on 6 July, and produced a GOES X-class flare on July 9 – the first since 1992 – a few M-class flares, and many C-class flares, all over a period of only three days. According to Zirin (1996), the region erupted as a dynamic emerging flux region (EFR) on 6 July. Additional loops emerged over the next few days and a delta spot had formed on 8 July. The region subsequently produced an M1.4 flare and an X2.6 flare on 9 July (Dryer *et al.*, 1998). Activity began to decrease after these events with no more M-class flares following an M1 flare on 10 July. Two

*NRC–MSFC Research Associate.

Solar Physics **201:** 71–91, 2001.

umbrae in the delta spot disappeared, leaving a normal bipolar region behind. The region itself however continued to persist in a quiet state for several solar rotations.

Thus the region progressed from a quiescent complex of activity, experienced a phase of greatly enhanced activity in conjunction with the presence of an EFR, and then entered an extended quiescent phase. Our objective in this paper is to examine the energy output of this region due to flaring activity during its active phase, and compare it with the energy output by the region during both the times inbetween flares in the active EFR period and the quiescent times preceding and following the active period. We can use our results to test the validity of identifying active-region emission with flare-like activity. This theoretically attractive 'nanoflare' hypothesis (Parker, 1989; Sturrock *et al.*, 1990) has been challenged by observations. Statistical studies of flares and microflares (Dennis, 1985; Hudson, 1991; Shimizu, 1995) found that input energy into flares was about an order of magnitude less than energy required to maintain a non-flaring active region, and Hudson (1991) pointed out that the distribution of flare energies implies energetic domination by large events, not small ones.

The sulphur channel of *Yohkoh* Bragg Crystal Spectrometer (BCS) has proved capable of observing single active regions on the solar disk during non-flaring phases (Watanabe *et al.*, 1995; Sterling 1997a, b; Sterling, Hudson, and Watanabe, 1997). The BCS has no spatial resolution, but during solar minimum a single active region can dominate the signal. The emissivity contribution curve of the resonance line of helium-like sulphur (S XV) is suitable for sensing high temperature components in active regions. The line-ratios of the resonance line, line *w* in the notation of Gabriel (1972), to the dielectronic satellites (q, j, and k) determine electron temperatures of $2.5-18\times10^6$ K, above which the blend with the forbidden line (z) impedes the temperature diagnostic capability of the sulphur lines in this wavelength range (Harra-Murnion, Akita, and Watanabe, 1996; Yuda *et al.*, 1997).

This paper describes the energetics of the active region NOAA 7978 and its successor on the subsequent rotation (NOAA 7981), as deduced from the helium-like sulphur observations of the *Yohkoh* BCS, and compares these results with observations from the Coronal Diagnostic Spectrometer (CDS) on board the Solar and Heliospheric Observatory (SOHO).

2. S xv Observation

The active region NOAA 7978 was the only conspicuous active region on the solar disk during the second week of July 1996. Following the emerging flux activity on 6 July, the soft X-ray intensity measured in the 1–8 Å channel of the GOES satellite increased from below A to middle B class, more than 1.5 orders of magnitude, in two days (see Figure 1).

The earliest available data in the Yohkoh BCS sulphur channel were those obtained after 18:00 UT on 7 July. Before this time, spectroscopic signals in the

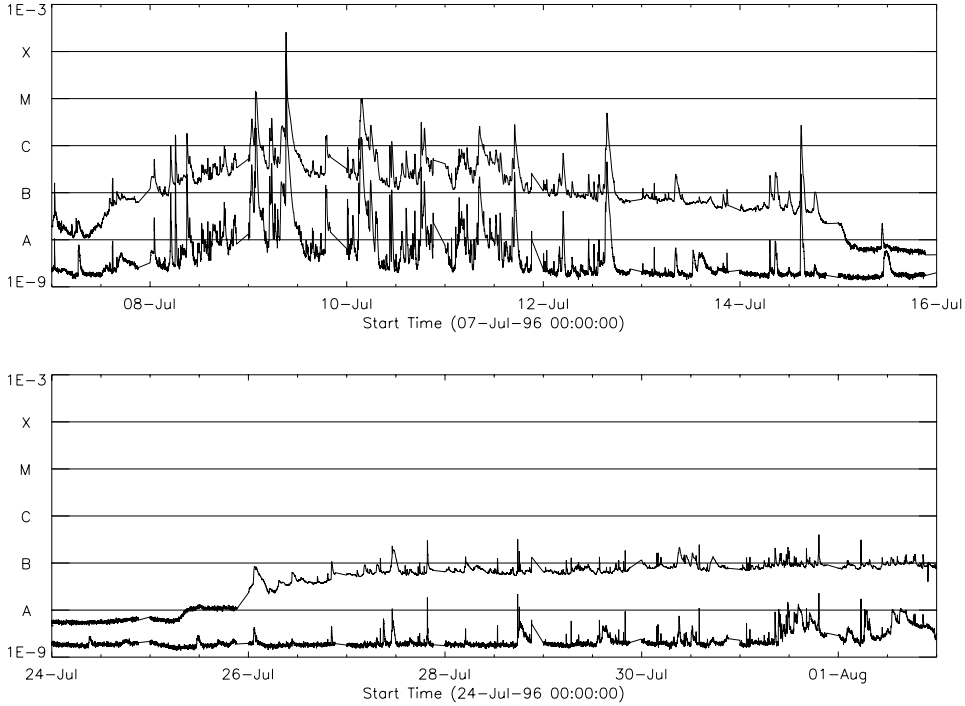

Figure 1. GOES-9 intensity plot for the first and second rotations of the active region NOAA 7978/7981.

channel were weak and lost in the background (Sterling, Hudson, and Watanabe, 1997). We applied standard BCS analysis techniques with a single-component synthetic spectral fit to the available data through the end of 12 July, using a fixed integration time interval of 240 s. These 4-min integrations generally resulted in total counts $\gtrsim$ 10 000, ensuring reasonable spectral fits (Sterling, 1997a). Figure 2(a) shows the electron temperatures and emission measures obtained based on this analysis. Fragmentary data intervals of less than 4 min due to gaps in the observations are not used in the analysis.

In order to derive electron temperatures and emission measures averaged over the entire active region in the absence of discrete flaring activity, we extracted data points around the local minima of S XV and GOES 1–8 Å flux light curves in Figure 2(b). Corresponding to the rapid growth of the active region during the time of magnetic flux emergence, the average sulphur temperature increased from 4×10^6 K at around 18:00 UT on 7 July to 5.5×10^6 K at around 12:00 UT on 8 July (cf., Figure 2(b)). The same trend is seen in emission measure; it increased from 3×10^{47} cm^{-3} to 5×10^{47} cm^{-3} during the same period. The average temperatures and emission measures subsequently decreased to 3.8×10^6 K and 4×10^{47} cm^{-3}, respectively, by the end of 12 July.

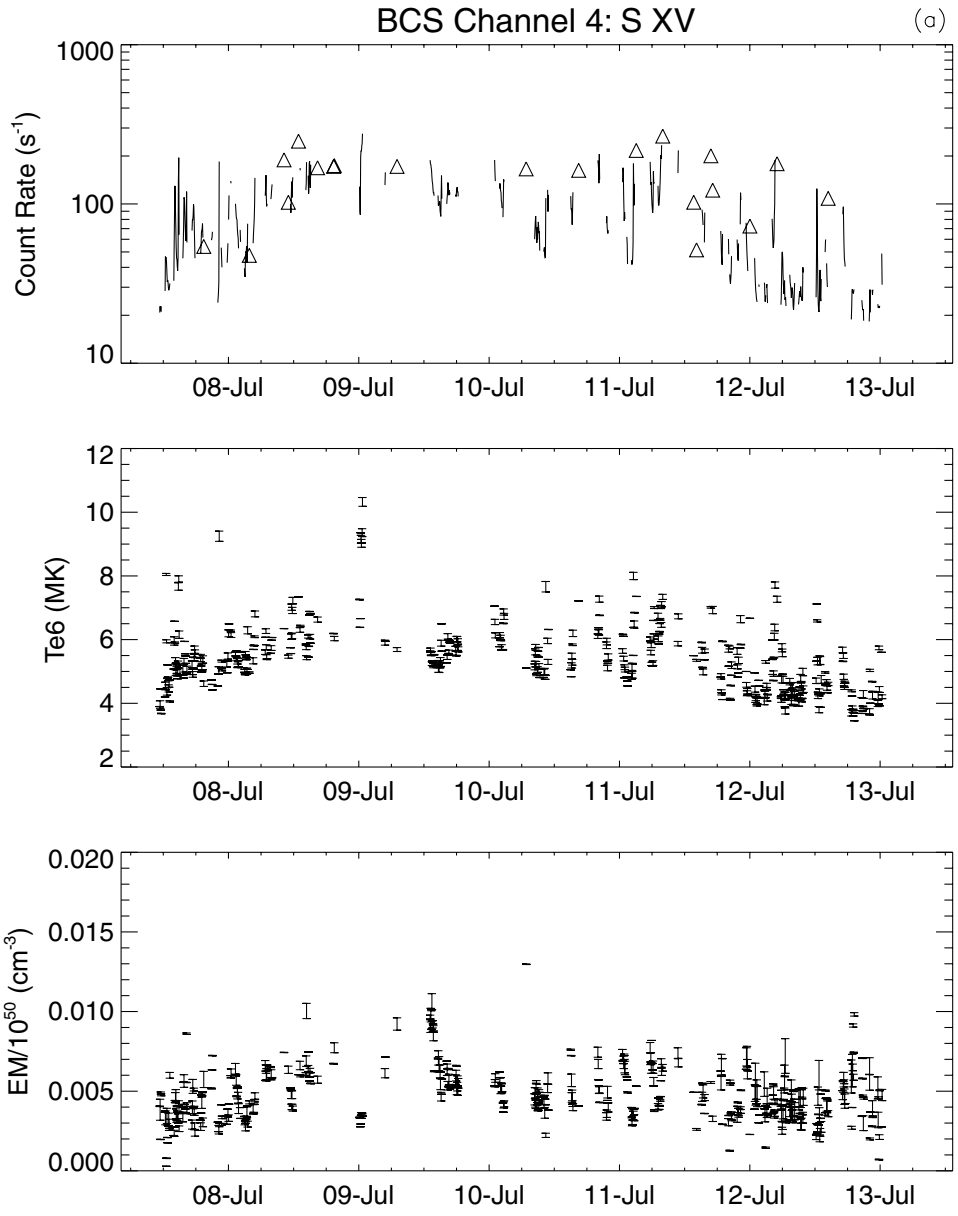

Figure 2a

Figure 2. (a) Single temperature and emission measure analysis of BCS S XV channel for the data obtained during 7–12 July 1996. (b) The same figure for the local minima of GOES and S XV line intensities during the same period.

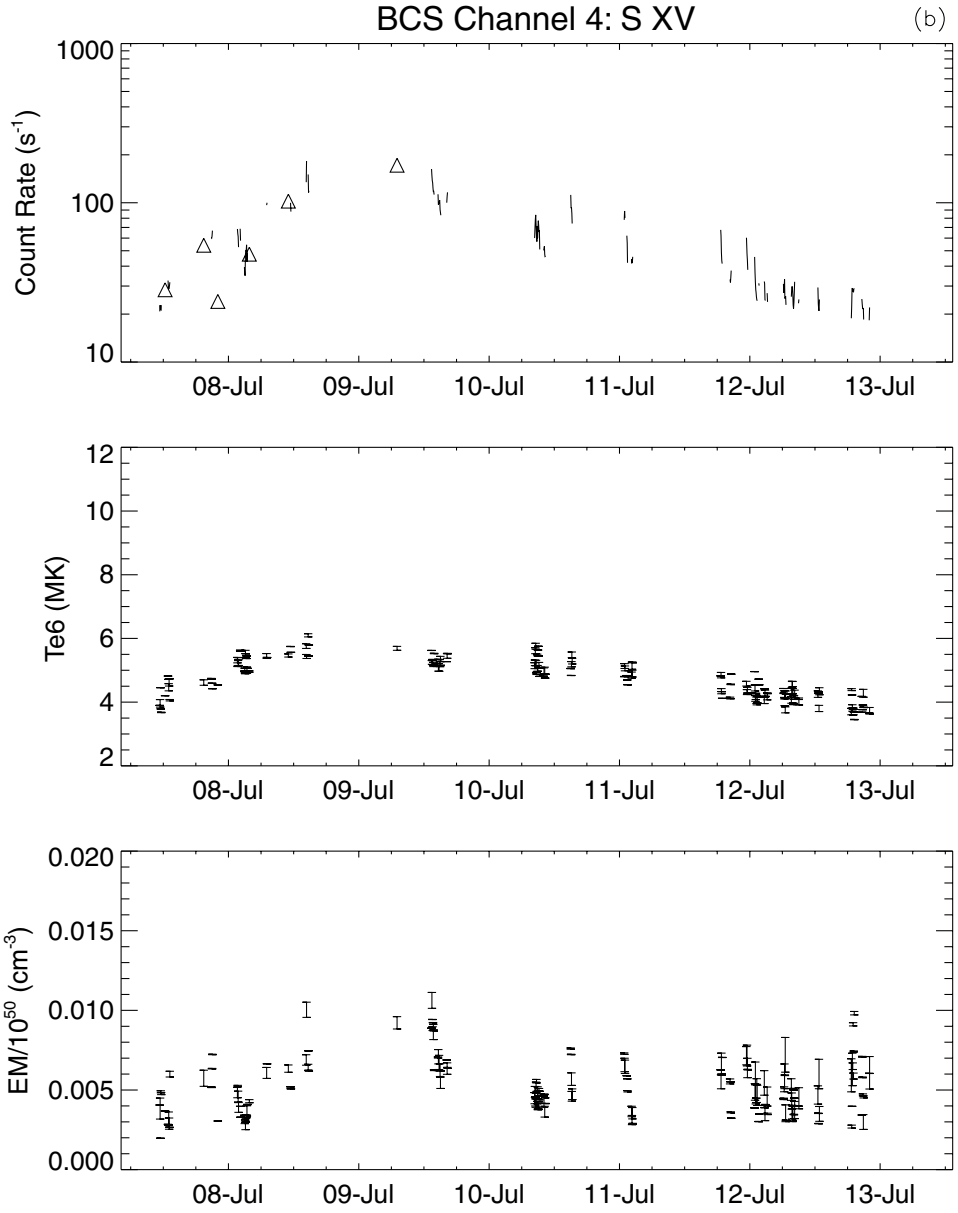
BCS Channel 4: S XV
(b)
Count Rate (s-1)
1000
100
10
08-Jul
09-Jul
10-Jul
11-Jul
12-Jul
13-Jul
Te6 (MK)
12
10
8
6
4
2
EM/1050 (cm-3)
0.020
0.015
0.010
0.005
0.000

Figure 2b.

After 12 July, flaring activity in this active region died away, with only one C-class flare on the 14th before the region rotated past the west limb on 15 July. The region reappeared on the earthward hemisphere on 26 July with new designation NOAA 7981; at that time its non-flaring level of soft X-rays remained nearly the same as when it had disappeared over the west limb a fortnight earlier. Moreover, flaring activity remained low, at a rate of several B-class flares per day.

The same analysis was applied to the data of 1 August as shown in Figure 3(a). From this dataset, we select out the data when the region NOAA 7981 is quietest by excluding the flaring enhancements. This limited dataset and the corresponding data analysis results are shown in Figure 3(b). From the non-flaring data of Figure 3(b), we find electron temperatures and emission measure of $(3.9 \pm 0.3) \times 10^6$ K and $(6 \pm 1) \times 10^{47}$ cm^{-3}, respectively, averaged over the whole day.

3. Radiative Energy Balance

In this section, we estimate the active region's thermal energy based on radiative loss considerations. We will make this estimate separately for the flaring component and the non-flaring components of the active region. The implication of the relationship to the total energy of the active region and the estimation of conductive fluxes obtained from CDS observations are discussed in the following section.

We first consider the thermal energy in the flares, using the events logged in the GOES event list. These events are given in Table I, as reported in *Solar Geophysical Data* (*SGD*) for the GOES-7 spacecraft. It is not possible to measure the temperatures and emission measures for all of these events, since *Yohkoh* could not observe many of them due to spacecraft night and other data gaps. Instead, we estimate the temperatures and emission measures of the listed flares from the GOES-class levels by using plots of temperature and emission measure vs. GOES-class determined by Yuda *et al.* (1997). Background levels are determined by visual inspection in applying the Yuda *et al.* fits. Table I gives the resulting temperatures (T_e) and emission measures (EM) determined in this fashion. The BCS S XV channel saturates at higher flux levels, and so the Yuda *et al.* results are based on flares in the GOES-class A – C range. We have extrapolated their results to flares of M- and X-class in Table I.

The thermal energy, $E_{th} (= 3kTn_eV$, where k is Boltzmann constant), can be estimated from our derived T and EM, where $EM = n_e^2 V$, via

$$E_{th} = P(T) \times EM \times t \quad \text{and} \quad n_e = (3kT \times EM)/E_{th} \,, \tag{1}$$

where the radiative loss power $P(T) = \chi T^{-1/2}$ (erg cm^3 s^{-1}) with $\chi \sim 10^{-18.81}$ for $T_e \gtrsim 10^{-5.5}$ K (Raymond and Smith, 1977), and t is the flare duration listed in *SGD*.

Our results are given in Table I. Here, the decay times of flares are simply assumed to represent radiative time scales with no post-flare heating. Nonetheless,

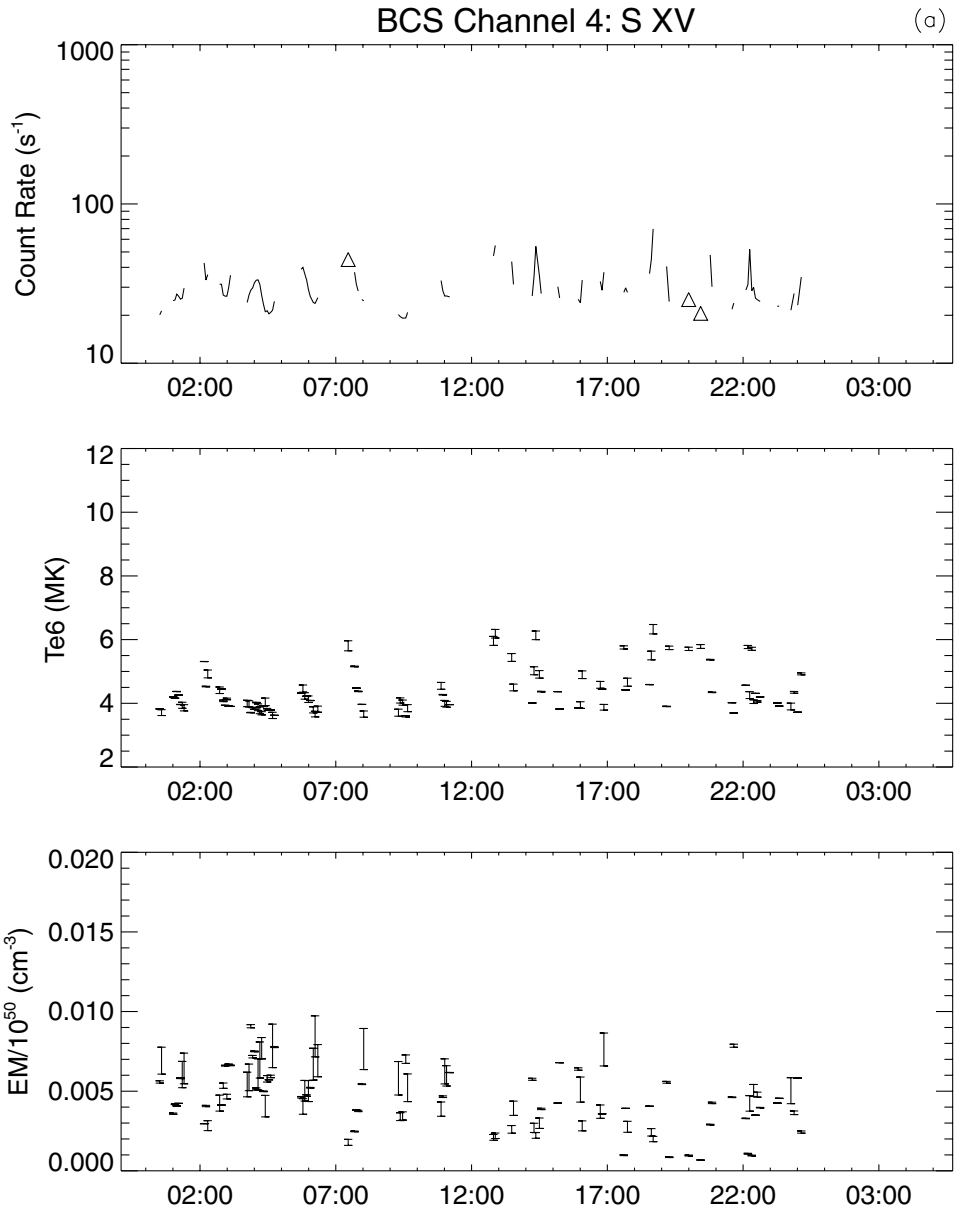

Figure 3a

Figure 3. (a) Single temperature and emission measure analysis of BCS S XV channel during 1 August 1996. (b) The same figure for the local minima of GOES S XV line intensities during the same period.

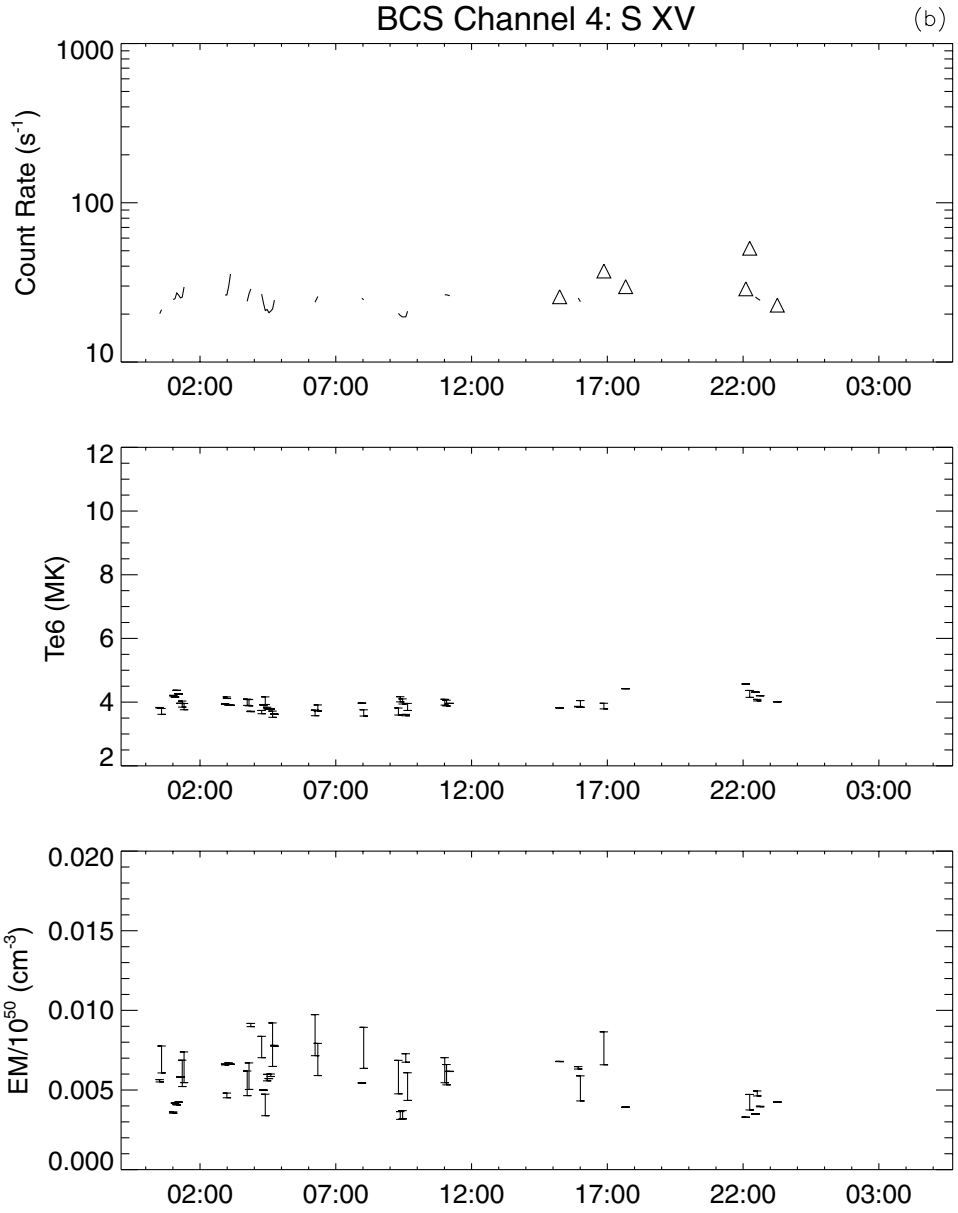
BCS Channel 4: S XV
(b)
Count Rate (s-1)
1000
100
10
02:00
07:00
12:00
17:00
22:00
03:00
Te6 (MK)
12
10
8
6
4
2
EM/1050 (cm-3)
0.020
0.015
0.010
0.005
0.000

Figure 3b.

TABLE I

Energy input via flares and energy yield of active region

Date	Begin	End	Δt	GOES	BG	Net	log T_e	log EM	TEC	n_e	E_{input}	$\text{Sum}_{1/4\text{day}}$	Sum_{day}	log T_e	log EM	TEC	n_e
8 July	00:20	00:46	26	B2.2	A9	B1.3	6.88	47.52	1.07(39)	4.22(10)	2.52(28)			6.60	47.48	5.00(38)	8.40
	01:01	01:06	6	B5.1	A9	B4.2	6.92	47.92	2.95(39)	2.14(11)	1.38(28)						
	03:30	03:42	12	B1.3	A9	A4	6.84	47.11	3.83(38)	7.82(10)	4.90(27)						
	04:31	05:08	37	C1.0	B1.0	B9.0	6.95	48.18	5.72(39)	3.84(10)	1.49(29)	1.93(29)					
	06:09	06:25	16	C1.6	B1.5	C1.5	6.97	48.34	8.65(39)	9.47(10)	9.14(28)						
	08:58	09:09	11	C1.8	B1.5	C1.7	6.97	48.39	9.68(39)	1.40(11)	6.91(28)	1.60(29)					
	12:31	12:50	19	B3.9	B1.7	B2.2	6.90	47.70	1.68(39)	6.20(10)	2.72(28)						
	14:05	14:11	6	B5.0	B2.0	B3.0	6.91	47.80	2.20(39)	2.05(11)	1.08(28)						
	15:19	15:26	7	B4.1	B1.9	B2.2	6.90	47.70	1.68(39)	1.68(11)	1.00(28)						
	16:20	16:25	5	B3.6	B2.1	B1.5	6.89	47.57	1.21(39)	2.24(11)	5.39(27)						
	16:58	17:13	15	B5.8	B2.4	B3.4	6.92	47.85	2.46(39)	8.32(10)	2.95(28)						
	17:44	17:50	6	B4.1	B2.4	B1.7	6.89	47.61	1.35(39)	1.90(11)	7.09(27)	8.99(28)					
	18:06	18:13	7	B8.9	B2.4	B6.5	6.94	48.07	4.31(39)	1.94(11)	2.22(28)						
	18:19	18:45	21	B4.5	B3.2	B1.3	6.88	47.52	1.07(39)	5.23(10)	2.04(28)						
	20:30	20:37	7	B7.0	B3.2	B3.8	6.92	47.88	2.71(39)	1.81(11)	1.49(28)						
	21:34	22:21	47	C4.8	B4.7	C4.3	7.01	48.72	2.24(40)	3.73(10)	6.00(29)						
	23:39	23:45	6	B7.9	B3.3	B4.6	6.93	47.95	3.19(39)	2.17(11)	1.47(28)	6.72(29)	1.11(30)	6.74	47.7	1.14(39)	8.63
9 July	00:18	01:04	46	C3.7	B4.3	C3.3	7.00	48.62	1.75(40)	3.67(10)	4.77(29)						
	01:49	02:21	32	M1.4	B8.0	M1.3	7.04	49.10	5.88(40)	6.35(10)	9.26(29)						
	05:03	05:53	50	C3.8	B3.3	C3.5	7.00	48.64	1.85(40)	3.40(10)	5.42(29)	1.95(30)					
	06:24	06:35	11	B8.2	B4.3	B3.9	6.92	47.89	2.77(39)	1.16(11)	2.39(28)						
	07:05	07:26	21	B5.8	B3.3	B2.5	6.91	47.74	1.88(39)	5.71(10)	3.30(28)						
	07:51	08:53	62	C2.6	B4.3	C2.2	6.98	48.48	1.23(40)	2.58(10)	4.76(29)						
	09:01	09:49	48	X2.6	B2.2	X2.6	7.15	50.12	7.81(41)	6.30(10)	1.24(31)	1.29(31)					
	18:49	19:35	46	C1.7	B2.4	C1.5	6.97	48.34	8.70(39)	3.30(10)	2.64(29)						
	22:21	22:27	6	B6.2	B2.0	B4.2	6.92	47.92	2.95(39)	2.14(11)	1.38(28)						
	22:29	22:54	25	C5.0	B2.0	C4.8	7.01	48.75	2.45(40)	7.11(10)	3.44(29)	6.22(29)	1.55(31)				

TABLE I
Continued

Date	Begin	End	Δt	GOES	BG	Net	log T_e	log EM	TEC	n_e	E_{input}	$\text{Sum}_{1/4\text{day}}$	Sum_{day}	log T_e	log EM	TEC	n_e
10 July	00:10	00:32	22	B9.4	B2.6	B6.8	6.94	48.08	4.48(39)	6.22(10)	7.20(28)						
	01:26	01:45	19	B4.7	B2.0	B2.7	6.91	47.77	2.01(39)	6.37(10)	3.16(28)						
	03:30	03:34	4	M1.0	B1.9	C9.8	7.03	49.00	4.55(40)	4.89(11)	9.31(28)						
	05:44	06:04	20	C2.7	B8.0	C1.9	6.98	48.43	1.09(40)	7.85(10)	1.39(29)	3.36(29)					
	10:29	10:42	13	B9.8	B1.3	B8.5	6.95	48.16	5.44(39)	1.09(11)	5.01(28)						
	10:57	11:14	17	C1.2	B1.3	C1.1	6.96	48.24	6.65(39)	8.56(10)	7.77(28)	1.28(29)					
	13:30	13:40	10	B4.5	B1.2	B3.3	6.92	47.84	2.39(39)	1.24(11)	1.92(28)						
	14:28	15:10	42	B7.2	B5.1	B2.1	6.90	47.68	1.62(39)	2.79(10)	5.80(28)						
	16:38	16:44	6	B6.6	B2.0	B4.6	6.93	47.95	3.19(39)	2.17(11)	1.47(28)	9.20(28)					
	18:04	18:26	22	C3.1	B1.6	C2.9	6.99	48.58	1.60(40)	7.57(10)	2.11(29)						
	18:48	19:05	17	C2.2	B2.4	C2.0	6.98	48.45	1.12(40)	9.28(10)	1.21(29)						
	19:51	20:06	15	B5.8	B2.4	B3.4	6.92	47.85	2.46(39)	8.32(10)	2.95(28)						
	21:02	21:15	13	B5.4	B2.4	B3.0	6.91	47.80	2.20(39)	9.44(10)	2.33(28)						
	22:43	22:58	15	C1.5	B4.9	C1.0	6.96	48.22	6.32(39)	9.62(10)	6.57(28)	4.51(29)	1.01(30)				
11 July	23:59	00:08	9	B1.7	B1.2	A5	6.85	47.19	4.65(38)	1.07(11)	4.33(27)						
	01:32	01:38	6	B2.5	B1.2	B1.3	6.88	47.52	1.07(39)	1.83(11)	5.83(27)						
	02:36	02:40	4	B3.4	B1.2	B2.2	6.90	47.70	1.68(39)	2.95(11)	5.72(27)						
	03:17	03:24	7	B6.2	B1.2	B5.0	6.93	47.98	3.43(39)	1.88(11)	1.83(28)						
	03:24	03:31	7	B9.0	B1.2	B7.8	6.95	48.13	5.05(39)	1.99(11)	2.53(28)						
	05:19	05:28	9	B8.7	B1.2	B7.5	6.95	48.12	4.88(39)	1.54(11)	3.17(28)	9.12(28)					
	07:00	07:10	10	B2.9	B1.2	B1.7	6.89	47.61	1.35(39)	1.14(11)	1.18(28)						
	08:08	08:40	32	C2.6	B1.5	C2.5	6.99	48.52	1.36(40)	5.08(10)	2.69(29)						
	10:52	11:07	15	B7.4	B3.8	B3.6	6.92	47.87	2.58(39)	8.39(10)	3.08(28)	3.11(29)					
	12:31	12:43	12	B8.4	B4.0	B4.4	6.93	47.93	3.07(39)	1.08(11)	2.85(28)						
	13:21	13:41	20	B7.1	B2.8	B4.3	6.93	47.93	3.01(39)	6.44(10)	4.68(28)						
	16:19	16:44	25	B5.4	B1.9	B3.5	6.92	47.86	2.52(39)	5.01(10)	5.02(28)						
	16:56	17:10	14	C2.8	B1.1	C2.7	6.99	48.55	1.48(40)	1.17(11)	1.26(29)	2.51(29)					
	21:04	21:12	8	B2.5	B1.1	B1.4	6.89	47.54	1.14(39)	1.39(11)	8.20(27)						
	22:18	22:34	16	C1.2	B1.1	C1.1	6.96	48.24	6.75(39)	9.11(10)	7.41(28)	8.23(28)	7.36(29)				

TABLE I

Continued

Date	Begin	End	Δt	GOES	BG	Net	log T_e	log EM	TEC	n_e	E_{input}	$\text{Sum}_{1/4\text{day}}$	Sum_{day}	log T_e	log EM	TEC	n_e
12 July	00:46	00:52	6	B1.9	A9	B1.0	6.88	47.43	8.49(38)	1.77(11)	4.80(27)			6.58	47.6	6.27(38)	8.36
	02:31	02:37	6	B1.5	A9	A6	6.86	47.25	5.45(38)	1.65(11)	3.30(27)						
	04:37	04:59	22	B7.1	A8	B6.3	6.94	48.06	4.20(39)	6.16(10)	6.81(28)	7.62(28)					
	06:57	07:16	19	B1.2	A8	A4	6.84	47.11	3.83(38)	4.94(10)	7.76(27)						
	10:55	11:11	16	B2.5	A7	B1.8	6.90	47.63	1.41(39)	7.17(10)	1.97(28)	2.75(28)					
	12:18	12:27	9	B1.7	A7	B1.0	6.88	47.43	8.49(38)	1.18(11)	7.21(27)						
	13:17	13:35	18	B2.2	A6	B1.6	6.89	47.59	1.28(39)	6.27(10)	2.04(28)						
	15:13	16:31	78	C4.9	A6	C4.84	7.01	48.75	2.46(40)	2.28(10)	1.08(30)	1.11(30)	1.21(30)				

Remark: Δt is the flare duraton in minutes. BG is the background level of the solar signal in GOES notation. Net is GOES-BG, net flare GOES flux. TEC stands for thermal energy content defined as $3\,KT \times EM$. The last four columns show the same quantities for the stationary component of the active region at the three epochs indicated in the same rows. See the text.

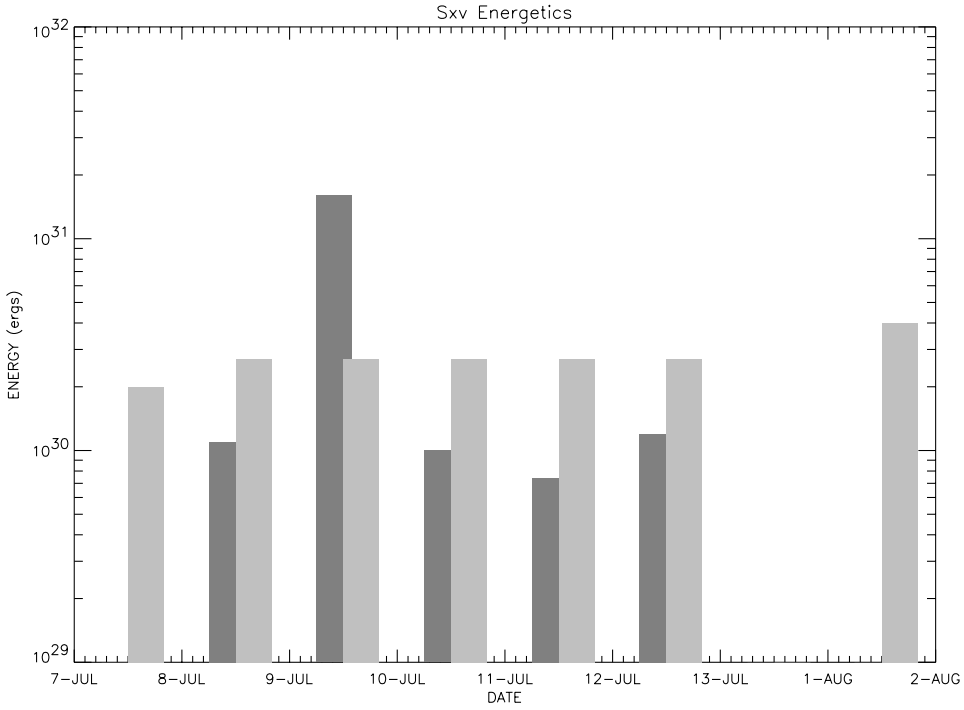

Figure 4. Energy balance of AR NOAA 7978. *Dark bars* and *gray bars* indicate daily energy expenditure in flares and background AR corona, respectively.

our estimated electron densities fall in the range 10^{10-11} cm^{-3}, which covers values often derived from more detailed analyses of individual flares. We therefore have confidence that our approximate approach is adequate.

We take the flare thermal energy as a measure of thermal energy input into the active region. The listed events are the flares greater than B1, but recent frequency analyses of flare occurrence (Dennis, 1985; Shimizu, 1995) show that if the distribution continues down to microflares, the integrated total energy from flares is still largely determined by the bigger flares, as the negative power index of the distribution as a function of energy is 1.5–1.6 (Hudson, 1991).

We next determine the energy needed to maintain the 'background' active region, that is, the energy liberated by radiation from the non-flaring active region over one day. We derived this using Equation (1), where the input T and EM are from the S XV results shown in Figure 2(b).

For the first five days following the rapid growth of the active region, we find the flare energy to be comparable to or in excess of the energy required to maintain the background active region. The comparison in Figure 4 might be taken to imply that the energy in flare activity is comparable to the heating of an active region during such a period. However, there is no one-to-one correspondence between changes in temperature and emission measure of the active region with flare activity; further-

more, during the second rotation of the active region, no flares above C1 occurred, even though the thermal yield of the background active region was comparable to that found during the first rotation.

These facts suggest that the the non-flaring active region plasmas detected in S XV originate from a different heating mechanism from that for the flaring plasmas. This is consistent with previous studies indicating that active-region coronae consist of two components, viz., a hotter, transient component and a cooler, more steady component (Watanabe *et al.*, 1995; Yoshida and Tsuneta, 1996; Sterling, Hudson, and Watanabe, 1997). For example, using images from the *Yohkoh* Soft X-Ray Telescope (SXT), Yoshida and Tsuneta (1996) found that plasmas having above 5 MK originate from transient events and show temporal variations, while the lower-temperature (3–5 MK) plasmas show more stationary nature. Both components are also discernible in BCS (Sterling, Hudson, and Watanabe, 1997).

It is interesting to note that flares were observed during the first three rotations, while CME events from this active region occurred from its emergence throughout its decay (van Driel-Gesztelyi *et al.*, 1999).

4. CDS Observation and Conductive Loss

The discussion so far has been based on the radiative properties of high-temperature coronal plasmas. Thus the above results assume that radiation is the major energy-loss term for coronal loops. If this were not the case, our conclusions would have to be modified. The other important mechanism which prevails in high-temperature plasmas is conductive loss to the lower atmosphere. The expansion of coronal loops may also consume a fraction of the active region energy, but we assume this to be substantially less than the radiative loss (Uchida *et al.*, 1992). Thus in this section we will investigate the contribution of conduction to the active region's energy budget.

Estimation of conductive loss introduces ambiguity in the analysis, because the detailed structure of the coronal loops is unknown. An apparently single loop may consist of a bundle of loops. The filling factors of active-region coronal loops have been discussed by several authors (e.g., Wolfson *et al.*, 1983; Dere, Bartoe, and Brueckner, 1984; Takahashi, 2000). Semi-empirically deduced conductive decay time scales in flares are usually shorter than radiative decay time scales (Moore *et al.*, 1980), but observed flares generally decay more slowly than indicated by the conductive time scale, and this may suggest that post-flare heating is taking place. The work of Takahashi (2000) provides an alternative resolution to the discrepancy between observations and the calculated rates. He found an apparent pressure imbalance between the footpoints and the loop tops of 59 impulsive flares observed by *Yohkoh* SXT. This non-physical pressure imbalance can be made to disappear, if an appropriate filling factor in the loop cross section is assumed. It turns out that the necessary filling factor increases the calculated conduction cooling time

TABLE II
Emission measures observed in CDS and *Yohkoh*

Ion	T_i(MK)	Δ log T_i	log EM_{10}	log A_{10}	log EM_{27}	log A_{27}
O III	0.10	0.4	45.78	18.45	45.42	18.30
O V	0.22	0.3	46.61	19.67	46.02	18.19
Mg IX	0.89	0.2	47.59	18.97	47.40	18.69
Si XII	1.78	0.3	47.43	18.68	47.57	18.74
Fe XIV	1.78	0.2	47.94	18.84	47.98	18.76
Fe XVI	2.24	0.3	48.45	18.90	48.29	18.67
S XV	3.8–4.0	–	47.5	–	47.8	–

$_{10}$ = 10 July, $_{27}$ = 27 July, A is the active-region area in cm^2.

so that it is comparable to the radiative cooling time. An attempt to differentiate between possible postflare heating and a filling factor less than unity is beyond the scope of the present discussion; we will proceed assuming that the postflare heating contribution to the energy balance is not important.

We have used CDS observations on 10 and 27 July 1996 (see Figures 5(a) and 5(b)) to estimate the global properties of conductive flux from the active-region (NOAA 7978/7981) corona down to the transition region and chromosphere. The details of the instrument have been given elsewhere (Harrison *et al.*, 1996). The pixel size corresponds to 2.03 arc sec × 1.63 arc sec, and the total intensities of the emission lines given in Table II are obtained by summing flux inside the half-peak-intensity contours. Volume emission measures were derived with help of the ADAS code (Summers, 1994). No systematic changes in intensity were recognized between these dates, except in the O V line. We attribute this to variability in the transition region (Harrison *et al.*, 1997; Brekke, Kjeldseth-Moe, and Harrison, 1997). It has been known since *Skylab* that in active regions the cool transition-region loops have a shorter lifetime than the hot coronal loops (Sheeley, 1980). The cool loops were found to lie at the same altitudes as the hot loops and this has been confirmed by SOHO observations (e.g., Matthews and Harra-Murnion, 1997). The hot and cool loops have very different characteristics. The cool loops are much more dynamic than the coronal loops (Harra-Murnion, Aktia, and Watanabe, 1999; Kjeldseth-Moe and Brekke, 1998). Using correlation techniques and Fourier methods, Matthews, Klimchuk, and Harra (2000) have shown that the transition region is made up of the traditional footpoints of hot loops as well as the dynamic high-lying loops as described above and seen clearly in Figure 5(b).

Thus, we can use these values to estimate the total conductive flux, if these lines are assumed to be produced via conductive flux from the corona. In the simple case, where this flux and pressure are assumed constant, from Dupree (1972), Withbroe and Gurman (1973), Mariska (1992),

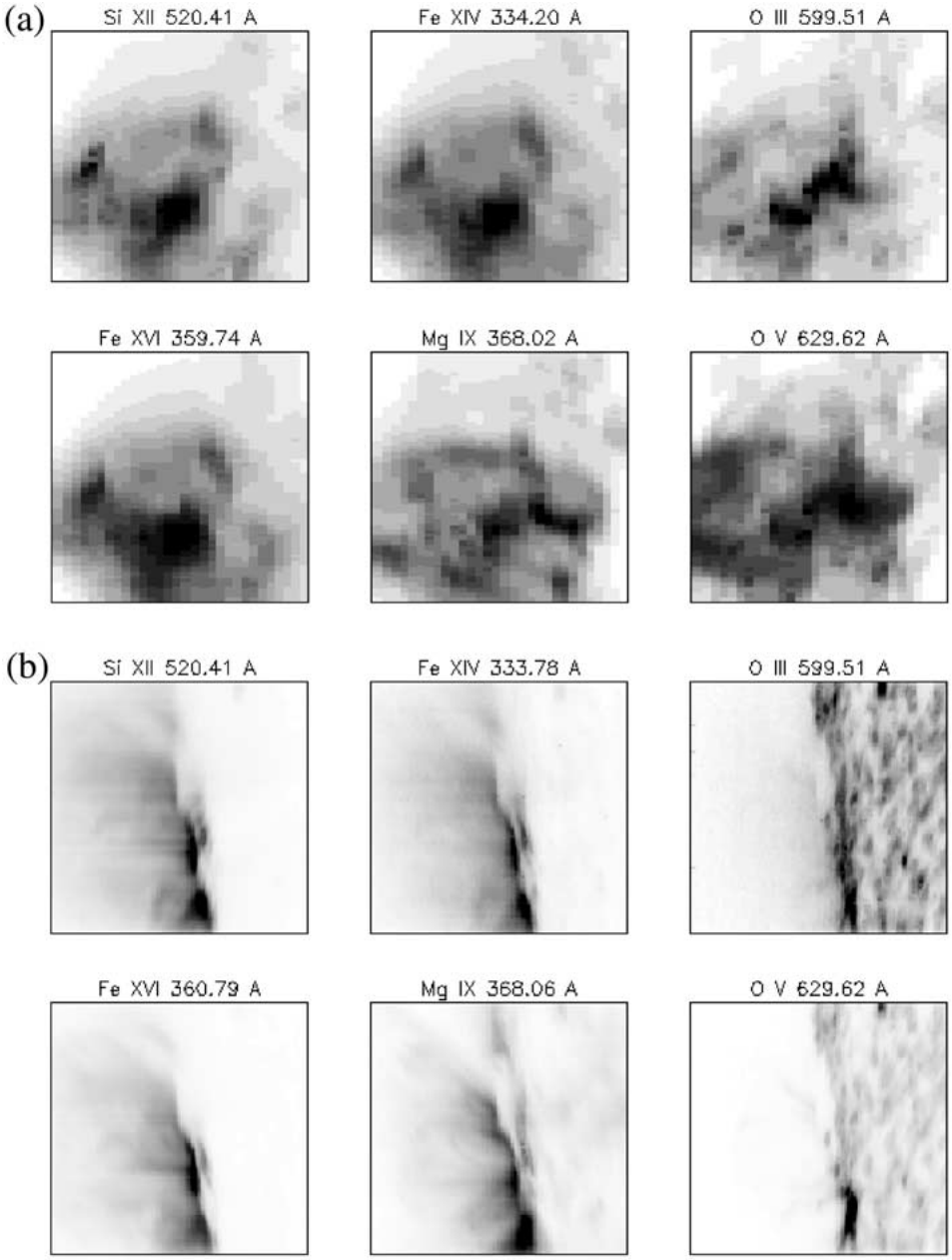

Figure 5. CDS images of AR NOAA 7978 on (a) 10 and (b) 27 July: observed areas are 122 arc sec × 119 arc sec in (a), and 244 arc sec × 240 arc sec in (b).

$$\int_R n_e^2 \mathrm{d}h = \frac{P^2}{4k^2T^2} \frac{\mathrm{d}h}{\mathrm{d}\log T} \Delta \log T \ , \tag{2}$$

and using

$$F_c/A = \kappa T^{5/2} \frac{\mathrm{d}T}{\mathrm{d}h} \ , \tag{3}$$

we can derive

$$F_c/p^2 \ = \ (A_i^2/EM_i)\ (\kappa/4k^2)\ T_i^{3/2}\ \Delta \log T_i \ , \tag{4}$$

where F_c is the total conductive flux from the active region corona, p is the pressure, A_i and EM_i are active region area and EM observed in line i, and T_i and $\Delta \log T_i$ are line-formation temperature and the width of its contribution curve, respectively. κ is the coefficient of thermal conductivity (Spitzer, 1962). In the case of active region NOAA 7978/7981, we find (Figure 6)

$$F_c/p^2 \ \approx \ 10^{24.41} \ , \tag{5}$$

(in c.g.s. units) where we have estimated A, T, and EM using least-squares fits to six lines covering the temperature range $0.1{-}2.2 \times 10^6$ K.

5. Energetics

We can now proceed to estimate the radiative and conductive contributions to the energy balance of the active region during the non-flaring times. We will do this by first assuming that the active region is composed of a set of coronal loops, where on average the loop-top temperature of these loops is the value derived from S XV. There were no drastic changes in line emission intensity and derived quantities seen on 10, 12, and 27 July and 1 August, so we use the average values for temperatures and emission measures from the S XV observations from these dates:

$$T_m \ \approx \ 10^{6.58}\ \mathrm{K} \quad \text{and} \quad EM \approx \ 10^{47.65}\ \mathrm{cm}^{-3} \ , \tag{6}$$

where T_m is the loop-top temperature. This implies

$$F_{\mathrm{rad}} = EM \times P(T) \ \approx \ 10^{25.49}\ \mathrm{erg\ sec}^{-1} \ , \tag{7}$$

where we have used the same form of $P(T)$ used in Equation (1).

We can obtain the total conductive flux of the active region with the observed active-region area A used in Equation (4),

$$A \ = \ 10^{18.96}\ \mathrm{cm}^2 \ , \tag{8}$$

which is the area observed in the CDS lines listed in Table II. No systematic changes of emitting area are found among the CDS lines observed at different line-of-sight angles (Figure 5). Assuming $V \sim A^{3/2}$ and the filling factor of unity, the pressure p and total conductive flux are estimated to

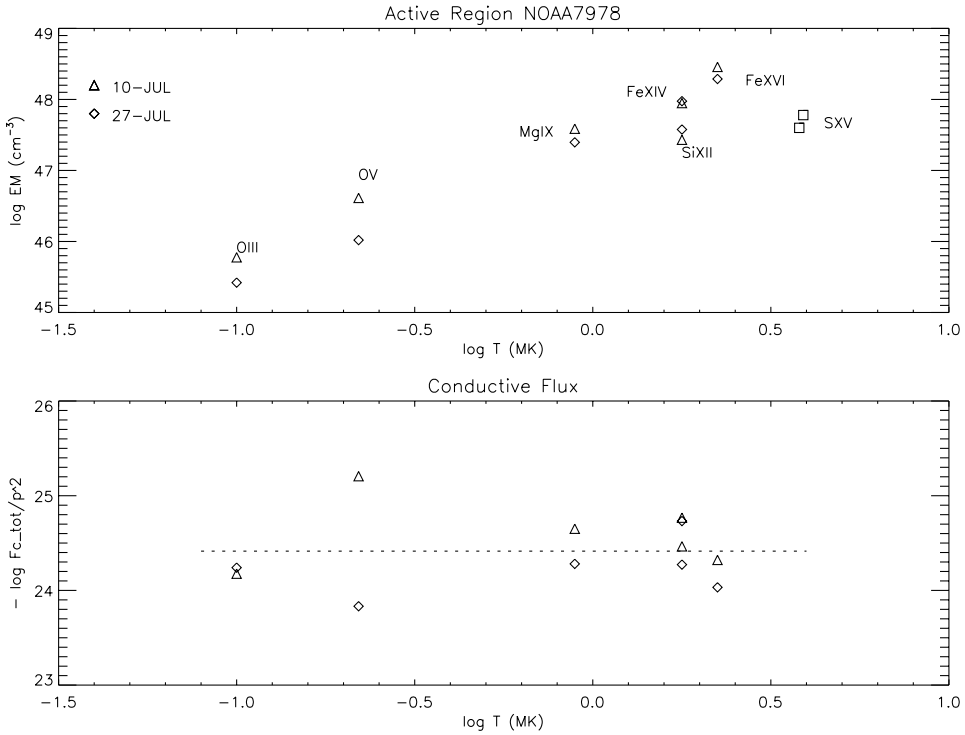

Figure 6. Emission measure plotted against line-formation temperature. *Dashed line* in the lower panel shows the estimate of conductive flux, F_c/p^2.

$$p \approx 10^{0.71} \text{ dyn cm}^{-2} \quad \text{and} \quad F_c \approx 10^{25.83} \text{ erg sec}^{-1} . \tag{9}$$

The total radiative loss of the entire active region estimated from S XV emitting plasmas is roughly equal to the total conductive loss downward to the transition-region and chromosphere.

We have now determined the pressure and total heat input of an average loop in the active region,

$$n_e T \approx 10^{16.27} \text{ K cm}^{-3} \quad \text{and} \quad f_{\text{tot}} \approx 10^{7.14} \approx 1.38 \times 10^7 \text{ erg cm}^{-2} \text{ sec}^{-1} , \tag{10}$$

where $f_{\text{tot}} = (F_{\text{rad}} + F_c)/A$.

In summary, estimates of radiative and conductive losses based on the observed sizes of the active region suggest that the radiative process is one of the major energy transfer processes in the active regions. Therefore, the energetics arguments presented in Section 3, based on the radiative losses alone, should be correct as an order-of-magnitude estimate. This is consistent with the idea that conductive losses will drive evaporation, increasing the loop density to a point of approximate equality of the loss terms (Cargill, Mariska, and Antiochos, 1995).

We can calculate the energy input, F_{rad} ($\sim F_{\text{tot}}$), over a full day due to both the flares of the active region and for the non-flaring component of the active region,

TABLE III

S XV energetics of active regions

Name	T_e^{a}	EM^{a}	$P_{\rm rad}\tau EM^{b,c}$	$E_{FL}/\tau^{c,d}$
NOAA 7260	5.7×10^6	3×10^{48}	1.8×10^{31}	1.5×10^{31}
NOAA 7978	4×10^6	4×10^{47}	2×10^{30}	1.5×10^{30}
NOAA 7981	4×10^6	4×10^{47}	2×10^{30}	5×10^{28}
NOAA 7953	5×10^6	1×10^{47}	5×10^{29}	3×10^{29}

[a]Non-flaring AR values. Values for ARs 7260, 7978, and 7953 are background values (i.e., in-between-flare values) during times when flare activity was high. AR 7981 values are from when flare activity was very low.
[b]Energy expenditure in flares (averaged over one day).
[c]$\tau = 86\,400$ s.
[d]Energy expenditure in background AR corona (averaged over one day).

that is, the energy flux needed to maintain temperature and emission measure of the non-flaring active region, as we did in obtaining Figure 4. These daily rate estimates are shown in Table III. The second row of Table III is for the active region NOAA 7978 in this paper: For the period of intense flare activity and flux emergence, the energy required per day to maintain the entire active region (the third column of Table III) is comparable to the energy of the active region's flare activity (the fourth column of the table, which gives the daily flare thermal energy estimated from the radiative losses).

The same comparison can be applied to the other two active regions analyzed by Shimizu (1995) and Sterling (1997a). Shimizu (1995) made a statistical analysis of microflares occurring in active region NOAA 7260 and compared their input energies with the total energies of the active regions. He estimated the total radiative loss of the active region in non-flaring state to be 2.1×10^{26} erg sec^{-1}, and he estimated radiative energy due to microflares in soft X-rays to be 1.8×10^{26} erg sec^{-1}; thus the values for the radiative energy were comparable in both cases. Shimizu (1995), however, compared this radiative energy input from microflares rather to conductive loss estimated from a rough dimension analysis and concluded that microflare energy input was incompatible for the entire active region heating. Sterling (1997) used the BCS S XV channel for a diagnostic analysis of an active region NOAA 7953, which was the only conspicuous active region on the solar disk in March 1996. Early in the observation period, the GOES light curve showed microflare activity, which subsequently substantially decreased, even though the region continued to live for several days. We estimated the energy of microflare activity for that region in the same way as we did for NOAA 7978/7981 in Section 3, using the GOES event list of flares. Information on S XV temperatures and emission measures of the active region was obtained from Figure 4 of Sterling (1997).

Table III summarizes our findings regarding energetics for NOAA ARs 7978/7981, 7260, and 7953. For AR 7978/7981, we have results for the flares and the background active-region corona both during times of high flaring and times of low flaring. For the other two regions we have results for the flares and the background active region during times of high flaring only. During times of high flaring the flare thermal energy is comparable to the thermal energy required to power the region in the absence of flares in all three regions. For region 7978/7981, however, during times of low flaring the thermal energy of the background corona is about the same as it had been when the flaring was intense, but the flare thermal energy is substantially reduced. This strongly suggests that the heating of the background active region is independent of the heating in the flares; it follows that the flares are not responsible for the heating of the background corona.

Further evidence that flare heating is independent of heating in the background corona comes from studies of preflare structures. Indeed most flares do not occur in previously illuminated flux tubes (Fárník, Hudson, and Watanabe, 1996), so that the two kinds of coronal heating involve distinctly different structures. And, as mentioned in the introduction, the heating of active regions also cannot be simply explained by the microflare hypothesis by extension of the occurrence frequency distribution of microflares down to the 'nanoflare' energy regime (Hudson, 1991; Shimizu, 1995).

Some evidence to the contrary, however, was presented by Shimizu and Tsuneta (1997), who found an intensity correlation between the magnitudes of the time variability and the intensities of the persistent corona. Yasuno *et al.* (2000) also made a statistical analysis of preflare-loop thermal characteristics, and found that the higher the temperatures of apparently steady-state preflare loops in active regions, the larger the flares they produce. These correlations all suggest that apparently stationary heating is closely related to transient heating in active regions, in conflict with results suggesting two completely independent heating mechanisms. Our findings in the present work are consistent with the flare and the stationary heating in active regions arising from different mechanisms, admitting that the flare thermal energy is of comparable order to the active region thermal energy during times of high-activity.

6. Conclusions

Comparing S XV observations by *Yohkoh* and lower-coronal and transition-region lines by CDS, we find that an average loop in active region NOAA 7978 has a loop-top temperature close to 4×10^6 K observed in S XV lines. We have deduced that the conductive loss downward to the chromosphere is nearly equal to radiative loss estimated at the loop-top. The pressure and the total heat input of the average loop in this active region are estimated to be $n_e T \approx 2 \times 10^{16}$ K cm^{-3} and

$f_{\rm tot} \approx 10^7$ erg cm^{-2} sec^{-1}, respectively. In contrast, a purely morphological analyses can overestimate the conductive fluxes (Shimizu, 1995).

Over the few days during which flux emerged in the region, energy associated with flares was comparable to the energy required to power the active region outside of flaring. Except for this correlation, however, there is no evidence for a causal connection between the flare energy release and the heating of the remainder of the active region, or between the flare energy released and the heating of the region outside of flaring times. The clearest evidence of this is that the steady heating of the background (i.e., non-flaring) active region both preceded and continued for many days after the period of the flare heating. For example, the non-flaring active region maintained approximately the same temperature and emission measure as it did during the non-flaring periods over the first two rotations, despite there being many flares during the first rotation but no flares bigger than C1 during the second rotation. This finding strongly argues against flare activity being the source of heating of the background active-region during the first two (and presumably subsequent) rotations. Therefore, if correct, the nanoflare hypothesis that tiny flare-like activity heats the entire solar corona would require that characteristics (occurrence frequency, energy distribution, etc.) of nanoflares be independent of the characteristics of larger discrete flares. For such larger flares, these characteristics seem rather universal over more than five orders of magnitude in flare size (Yuda *et al.*, 1997).

It is interesting to note that flares were observed only during the first three rotations of AR 7978 and its successors, while CME events from this region occurred from its emergence throughout its decay (van Driel-Gesztelyi *et al.*, 1999) in November 1996. This is also consistent with flares having a heating mechanism independent of that driving other processes in the region.

Our quantitative analysis of active region energetics via the S XV diagnostics confirms the need for both a steady heating mechanism and an independent mechanism for heating flares. This result confirms an obvious inference from X-ray light curves; sometimes the solar emission level recorded by GOES is dominated by flares, and sometimes not. For a given active region, we find that the flaring and the non-flaring components of the active region are energetically comparable during the growth phase, but differ by an order of magnitude in the decay phase.

Acknowledgements

TW is supported by the Japan Society for Promotion of Science for the UK–Japan Collaborative Scientific Programme. ACS holds an National Research Council–NASA/MSFC Research Associateship. LKH is grateful to PPARC for an Advanced Fellowship. TW and LKH are supported by the Royal Society for the Joint Research Programme. *Yohkoh* is operated by the science team in ISAS.

References

Brekke, P., Kjeldseth-Moe, O., and Harrison, R. A.: 1997, *Solar Phys.* **175**, 511.
Cargill, P. J., Mariska, J. T., and Antiochos, S.: 1995, *Astrophys. J.* **439**, 1034.
Culhane, J. L. *et al.*: 1991, *Solar Phys.* **136**, 89.
Dere, K. P., Bartoe, J. D. F., and Brueckner, G. E.: 1984, *Astrophys. J.* **281**, 870.
Dupree, A. K.: 1972, *Astrophys. J.* **178**, 527.
Dennis, B. R.: 1985, *Solar Phys.* **100**, 465.
Dryer, M. *et al.*: 1998, *Solar Phys.* **181**, 159.
Fárník, F., Hudson, H. S., and Watanabe, T.: 1996, *Solar Phys.* **165**, 169.
Gabriel, A. H.: 1972, *Monthly Notices Royal Astron. Soc.* **160**, 99.
Harra-Murnion, L. K. *et al.*: 1996, *Astron. Astrophys.* **308**, 670.
Harra-Murnion, L. K., Akita, K., and Watanabe, T.: 1997, *Astrophys. J.* **479**, 467.
Harrison, R. A. *et al.*: 1996, *Solar Phys.* **162**, 233.
Harrison, R. A. *et al.*: 1997 *Solar Phys.* **175**, 467.
Hudson, H. S.: 1991, *Astrophys. J.* **133**, 357.
Kano, R. and Tsuneta, S.: 1996, *Publ. Astron. Soc. Japan* **48**, 535.
Kjeldseth-Moe, O.: 2000, *Adv. Space Res.* **25**, 1713.
Kjeldseth-Moe, O. and Brekke, P.: 1998, *Solar Phys.* **182**, 73.
Mariska, J. T.: 1992, *Solar Transition Region*, Cambridge University Press, p. 168.
Matthews, S. A. and Harra-Murnion, L. K.: 1997, *Solar Phys.* **175**, 541.
Matthews, S. A., Klimchuk, J. A., and Harra, L. K., 2000, *Astron. Astrophys.* (submitted).
Moore, R. *et al.*: 1980, in P. A. Sturrock (ed.), *Solar Flares – A Monograph from Skylab Solar Workshop II*, Cororado Associated Press, Boulder, p. 341.
Parker, E. N.: 1988, *Astrophys. J.* **330**, 474.
Raymond, C. and Smith, B. W.: 1977, *Astrophys. J. Suppl.* **35**, 419.
Sheeley, N. R.: 1980, *Solar Phys.* **66**, 79.
Shimizu, T.: 1995, *Publ. Astron. Soc.* **47**, 251.
Shimizu, T. and Tsuneta, S.: 1997, *Astrophys. J.* **486**, 1045.
Spitzer, L.: 1962, *Physics of Fully Ionized Gases*, Interscience, New York, p. 144.
Sterling, A. C.: 1997a, *Astrophys. J.* **478**, 807.
Sterling, A. C.: 1997b, *Geophysical Res. Lett.* **24**, 2263.
Sterling, A. C., Hudson, H. S., and Watanabe, T.: 1997, *Astrophys. J.* **479**, L149.
Sturrock. P. A., Dixon, W. W., Klimchuk, J. A., and Antiochos, S. K.: 1990, *Astrophys. J.* **356**, L31.
Summers, H. P.: 1994, *Atomic Data and Analysis Structure (ADAS) User Manual*, JET-IR (94) 06.
Takahashi, M.: 2000, *Adv. Space Res.* **25**, 1833.
Uchida, Y. *et al.*: 1992, *Publ. Astron. Soc. Japan* **44**, L155.
van Driel-Gesztelyi, L. *et al.*: 1999, *Third Advances in Solar Physics Euroconference: Magnetic Fields and Oscillations, ASP Conf. Ser.* **184**, 302.
Watanabe, T., Hara, H., Shimizu, T., Hiei, E., Bentley, R. D., Fludra, A., Lang, J., Phillips, K. J. H., Pike, C. D., Bromage, B. J. I., and Mariska, J. T.: 1995, *Solar Phys.* **157**, 169.
Withbroe, G. and Gurman, J.: 1973, *Astrophys. J.* **183**, 279.
Wolfson, C. J., Doyle, J. G., Leibacher, J. W., and Phillips, K. J. H.: 1983, *Astrophys. J.* **269**, 319.
Yasuno, S., Hiei, E., Hara, H., and Watanabe, T.: 2000, *Adv. Space Res.* **25**, 1805.
Yoshida, T. and Tsuneta, S.: 1996, *Astrophys. J.* **459**, 342.
Yuda, S., Hiei, E., Takahashi, M., and Watanabe, T.: 1997, *Publ. Astron. Soc. Japan* **47**, 115.
Zirin, H.: 1996, private communication.